

Dependence of kinetic plasma waves on ion-to-electron mass ratio and light-to-Alfvén speed ratio

Daniel Verscharen,^{1,2*} Tulasi N. Parashar,³ S. Peter Gary⁴
and Kristopher G. Klein⁵

¹Mullard Space Science Laboratory, University College London, Holmbury House, Holmbury St. Mary, Dorking RH5 6NT, UK

²Space Science Center, University of New Hampshire, 8 College Road, Durham, NH 03824, USA

³School of Chemical and Physical Sciences, Victoria University of Wellington, Gate 7, Kelburn Parade, Wellington 6012, New Zealand

⁴Space Science Institute, 4765 Walnut St, Boulder, CO 80301, USA

⁵Lunar and Planetary Laboratory and Department of Planetary Sciences, University of Arizona, 1629 E University Blvd., Tucson, AZ 85719, USA

Accepted XXX. Received YYY; in original form ZZZ

ABSTRACT

The magnetization $|\Omega_e|/\omega_e$ is an important parameter in plasma astrophysics, where Ω_e and ω_e are the electron gyro-frequency and electron plasma frequency, respectively. It only depends on the mass ratio m_i/m_e and the light-to-Alfvén speed ratio c/v_{Ai} , where m_i (m_e) is the ion (electron) mass, c is the speed of light, and v_{Ai} is the ion Alfvén speed. Nonlinear numerical plasma models such as particle-in-cell simulations must often assume unrealistic values for m_i/m_e and for c/v_{Ai} . Because linear theory yields exact results for parametric scalings of wave properties at small amplitudes, we use linear theory to investigate the dispersion relations of Alfvén/ion-cyclotron and fast-magnetosonic/whistler waves as prime examples for collective plasma behaviour depending on m_i/m_e and c/v_{Ai} . We analyse their dependence on m_i/m_e and c/v_{Ai} in quasi-parallel and quasi-perpendicular directions of propagation with respect to the background magnetic field for a plasma with $\beta_j \sim 1$, where β_j is the ratio of the thermal to magnetic pressure for species j . Although their dispersion relations are largely independent of c/v_{Ai} for $c/v_{Ai} \gtrsim 10$, the mass ratio m_i/m_e has a strong effect at scales smaller than the ion inertial length. Moreover, we study the impact of relativistic electron effects on the dispersion relations. Based on our results, we recommend aiming for a more realistic value of m_i/m_e than for a more realistic value of c/v_{Ai} in non-relativistic plasma simulations if such a choice is necessary, although relativistic and sub-Debye-length effects may require an additional adjustment of c/v_{Ai} .

Key words: plasmas – solar wind – waves – relativistic processes – methods: numerical

1 INTRODUCTION

The conditions and properties of plasmas in the universe vary greatly, ranging from stellar cores to accretion discs, the intracluster medium, stellar winds, planetary magnetospheres, and laboratory plasmas (Russell 1993; Opher 1999; Marsch 2006; Uzdensky & Rightley 2014; Verscharen et al. 2019; Zhu et al. 2019). Some of these systems exhibit collisional relaxation timescales comparable to or greater than the collective timescales of the plasma. The Vlasov–Maxwell set of equations describes such weakly collisional or collisionless plasmas adequately (Hasegawa & Sato 2013). We write

the Vlasov equation for species j (e for electrons, i for ions) in dimensionless form as

$$\frac{\partial f_j}{\partial \tilde{t}} + \tilde{\mathbf{v}} \cdot \frac{\partial f_j}{\partial \tilde{\mathbf{x}}} + \frac{q_j}{q_i} \frac{m_i}{m_j} \left(\frac{c}{v_{Ai}} \tilde{\mathbf{E}} + \tilde{\mathbf{v}} \times \tilde{\mathbf{B}} \right) \cdot \frac{\partial f_j}{\partial \tilde{\mathbf{v}}} = 0, \quad (1)$$

where f_j is the distribution function of species j , q_j and m_j are the charge and mass of a particle of species j , c is the speed of light, $\tilde{t} \equiv t\Omega_i$ is the normalized time, $\tilde{\mathbf{v}} \equiv \mathbf{v}/v_{Ai}$ is the normalized velocity, and $\tilde{\mathbf{x}} \equiv \mathbf{x}\Omega_i/v_{Ai}$ is the normalized spatial coordinate. Here, we define the signed gyro-frequency of species j as

$$\Omega_j \equiv \frac{q_j B_0}{m_j c} \quad (2)$$

* E-mail: d.verscharen@ucl.ac.uk

and the Alfvén speed of species j as

$$v_{Aj} \equiv \frac{B_0}{\sqrt{4\pi n_j m_j}}, \quad (3)$$

where B_0 is the reference (background) magnetic field strength and n_j is the density of species j . In Eq. (1), we normalize the electric and magnetic fields to B_0 as $\tilde{\mathbf{E}} \equiv \mathbf{E}/B_0$ and $\tilde{\mathbf{B}} \equiv \mathbf{B}/B_0$, respectively.

Eq. (1) demonstrates the importance of the quantities m_i/m_j and c/v_{Ai} for the Lorentz-force term in Vlasov systems. Combining both quantities for a quasi-neutral two-species plasma with $n_i \approx n_e$, we define the magnetization of the plasma as the ratio

$$\frac{|\Omega_e|}{\omega_e} = \frac{v_{Ai}}{c} \sqrt{\frac{m_i}{m_e}}, \quad (4)$$

where

$$\omega_j \equiv \sqrt{\frac{4\pi n_j q_j^2}{m_j}} \quad (5)$$

is the plasma frequency of species j . Kinetic simulations suggest that the ratio $|\Omega_e|/\omega_e$ is an important parameter that controls the slope of observed particle spectra in, for example, pulsar wind nebulae, active galactic nuclei, and gamma-ray bursts (Cerutti et al. 2013; Melzani et al. 2014a,b).

Nonlinear computations such as particle-in-cell, Eulerian-Vlasov, and hybrid simulations have become standard tools to model astrophysical plasma systems (Lapenta 2012; Kunz et al. 2014; Markidis et al. 2014; Melzani et al. 2014a; Germaschewski et al. 2016; Pezzi et al. 2019). Computational constraints often prevent us from simulating realistic values for the multiple length scales and timescales involved in astrophysical plasma processes (Vásconez et al. 2014; Franci et al. 2015; Parashar et al. 2015b; Allanson et al. 2019; Cerri et al. 2019; Pecora et al. 2019; Pezzi et al. 2019; Verscharen et al. 2019; Matsukiyo et al. 2020). In the solar wind at 1 au (Matthaeus & Goldstein 1982; McComas et al. 2000; Marsch 2006; Klein & Vech 2019), for example, the energy-containing scale of the turbulence is of order $L \sim 10^6 \text{ km} \sim 10^{11} \text{ cm}$, while the Debye length of species j ,

$$\lambda_j \equiv \sqrt{\frac{k_B T_j}{4\pi n_j q_j^2}}, \quad (6)$$

is of order 10^4 cm for both electrons and protons, where k_B is the Boltzmann constant, and T_j is the temperature of species j . This scale separation by seven orders of magnitude makes it difficult to simulate the system of size L with a resolution of λ_j based on present numerical capabilities. Kinetic simulations with particle-in-cell and Eulerian Vlasov codes, therefore, mostly focus on kinetic effects by resolving the relevant spatial scales such as the j th species' inertial length

$$d_j \equiv \frac{c}{\omega_j} = \frac{v_{Aj}}{|\Omega_j|} \quad (7)$$

or gyro-radius

$$\rho_j \equiv \frac{w_j}{|\Omega_j|}, \quad (8)$$

where

$$w_j \equiv \sqrt{\frac{2k_B T_j}{m_j}} \quad (9)$$

is the thermal speed of species j . Kinetic simulations often need to resolve all timescales from the ion gyration ($\sim 1/\Omega_i$) up to the electron plasma oscillation ($\sim 1/\omega_e$). For example, the ordering of kinetic length scales in the solar wind (assuming $\beta_j \sim 1$) is

$$d_i \sim \rho_i \gg d_e \sim \rho_e \gg \lambda_e, \quad (10)$$

where

$$\beta_j \equiv \frac{8\pi n_j k_B T_j}{B_0^2} \quad (11)$$

is the plasma- β (i.e., the ratio of thermal pressure to magnetic pressure) of species j . Considering that

$$\frac{d_i}{d_e} = \sqrt{\frac{m_i}{m_e}} \quad (12)$$

and

$$\frac{d_e}{\lambda_e} = \sqrt{\beta_e} \frac{\omega_e}{|\Omega_e|}, \quad (13)$$

achieving this ordering of scales in simulations requires sufficiently large values for m_i/m_e and c/v_{Ai} . However, typical values of $|\Omega_e|/\omega_e$ used in fully kinetic studies of the solar wind are $|\Omega_e|/\omega_e \sim 0.1 - 1$ (Karimabadi et al. 2013; Saito & Nariyuki 2014; Parashar et al. 2015b,a; Grošelj et al. 2018; Parashar & Gary 2019; Roytershteyn et al. 2019), in contrast to the realistic values $|\Omega_e|/\omega_e \sim 10^{-3} - 10^{-2}$ (for example, see Verscharen et al. 2019, table 1). Therefore, it is important to understand and quantify the effects of artificially large values of $|\Omega_e|/\omega_e$ on the dynamics of the system. We study this particular question in the context of linear plasma waves as some of the most fundamental building blocks of plasma dynamics. Linear wave theory has the unique advantage that it yields exact numerical results under the assumption that the fluctuation amplitude is small, whereas nonlinear computations such as particle-in-cell simulations yield only approximate scaling relations. Therefore, linear theory provides a standard of comparison against which small-amplitude simulations can be tested. The goal of our work is to provide ground truth for such comparisons between nonlinear computations and linear theory, and to raise awareness for the inaccuracies from artificially decreasing m_i/m_e and c/v_{Ai} in nonlinear computations.

2 PLASMA WAVES IN LINEAR THEORY

We use the numerical code NHDS (Verscharen & Chandran 2018) to solve the kinetic dispersion relation in a quasi-neutral two-species plasma consisting of isotropic and non-drifting Maxwellian ions and electrons. The Maxwellian distribution for species j is given by

$$f_{0j} = \frac{n_j}{\pi^{3/2} w_j^3} \exp\left(-\frac{v^2}{w_j^2}\right), \quad (14)$$

where v is the velocity coordinate and w_j is the thermal speed as defined in Eq. (9). NHDS, like other solvers of the hot-plasma dispersion relation (Roennmark 1982; Gary 1993; Klein & Howes 2015), determines the non-trivial solutions to the wave equation,

$$\mathbf{n} \times (\mathbf{n} \times \mathbf{E}) + \epsilon \mathbf{E} = 0, \quad (15)$$

where $\mathbf{n} \equiv \mathbf{k}c/\omega$, \mathbf{E} is the Fourier transform of the electric field, \mathbf{k} is the wavevector, ω is the (complex) wave frequency,

$$\boldsymbol{\varepsilon} \equiv \mathbf{1} + \sum_j \boldsymbol{\chi}_j \quad (16)$$

is the dielectric tensor, and $\boldsymbol{\chi}_j$ is the contribution of species j to the susceptibility (for details, see Stix 1992). NHDS calculates the tensor $\boldsymbol{\chi}_j$ from the linearised Vlasov equation [see Eq. (1)], Maxwell's equations, and Eq. (14).

We set $\beta_i = \beta_e = 1$. We investigate the Alfvén/ion-cyclotron (A/IC) wave and the fast-magnetosonic/whistler (FM/W) wave in both quasi-parallel ($\theta = 0.001^\circ$) and quasi-perpendicular ($\theta = 89^\circ$) directions of propagation with respect to the background magnetic field \mathbf{B}_0 , where θ is the angle between \mathbf{k} and \mathbf{B}_0 . These waves are important normal modes in plasmas (Ofman 2010; Marsch & Verscharen 2011; Verscharen et al. 2012; Boldyrev et al. 2013; Yoon 2015; Comişel et al. 2016; Cerri et al. 2017; Wu et al. 2019; Zhu et al. 2019). We show solutions for the real part ω_r of the wave frequency and for its imaginary part γ as functions of the wavenumber k . We only plot solutions when $|\gamma| \leq \omega_r$. We normalize all length scales in units of d_i and all frequencies in units of Ω_i . In addition, we indicate the values of $kd_e = 1$ for the different mass ratios in units of kd_i .

2.1 Dependence on ion-to-electron mass ratio

We first investigate the dependence of the A/IC and FM/W dispersion relations on m_i/m_e . We fix the light-to-Alfvén speed ratio at $c/v_{Ai} = 10^4$ and vary m_i/m_e between 1836 (i.e., the realistic value for the proton-to-electron mass ratio, m_p/m_e) and 1 (i.e., the value for an electron-positron plasma). The magnetization, therefore, varies from $|\Omega_e|/\omega_e = 10^{-4}$ to $|\Omega_e|/\omega_e \approx 4 \times 10^{-3}$. In Fig. 1, we show the dispersion relations for the A/IC wave in quasi-parallel propagation for different values of m_i/m_e . Both the real part of the normalized frequency and its imaginary part do not vary significantly with m_i/m_e since the dispersion relation of the quasi-parallel A/IC wave is dominated by ion dynamics (unless $kd_i \ll 1$) and by the onset of ion-cyclotron damping. The cyclotron-resonance condition for particles of species j is given by

$$\omega_r = k_{\parallel} v_{\parallel} + n\Omega_j, \quad (17)$$

where v_{\parallel} is the speed of the resonant particles in the \mathbf{B}_0 direction, and n is the integer order of the cyclotron resonance. Cyclotron-resonant interactions are typically most efficient for $n = \pm 1$. Since the quasi-parallel A/IC wave is left-hand polarized, electrons cannot cyclotron-resonate with this wave through the otherwise most efficient $n = -1$ resonance. We note that the resonant cut-off of the dispersion relation for $\omega_r \rightarrow \Omega_i$ is also present in the cold-plasma limit (Stix 1992).

In Fig. 2, we show the dispersion relations for the A/IC wave in quasi-perpendicular direction of propagation. This mode shows a characteristic maximum in ω_r . Both the normalized frequency and the normalized wavenumber associated with this maximum decrease with decreasing m_i/m_e . On the other hand, the magnitude of the damping rate $|\gamma|/\Omega_i$ increases with decreasing m_i/m_e . With decreasing m_i/m_e ,

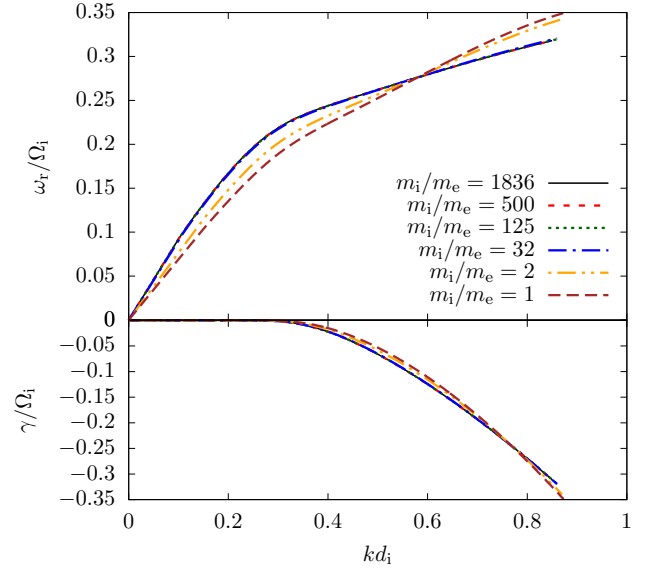


Figure 1. Dispersion relations of the A/IC wave in quasi-parallel propagation for different values of m_i/m_e . The light-to-Alfvén speed ratio is fixed at $c/v_{Ai} = 10^4$. The top panel shows the normalized real part of the wave frequency, and the bottom panel shows the normalized imaginary part of the wave frequency as functions of the normalized wavenumber k . None of the solutions reaches $kd_e = 1$ while $|\gamma|/\omega_r < 1$.

the electron thermal speed decreases, leading to a non-isothermal electron behaviour and an increase in the electron inertia. This effect becomes important for the quasi-perpendicular A/IC wave since it is a compressive mode at $k\rho_i \gtrsim 1$ (Schekochihin et al. 2009; Hunana et al. 2013; Chen & Boldyrev 2017). However, the behaviour of the quasi-perpendicular A/IC wave does not vary significantly over the explored m_i/m_e range at small $kd_i \lesssim 1$. For $m_i/m_e \lesssim 100$, the quasi-perpendicular A/IC mode damps heavily (i.e., $|\gamma| \gtrsim \omega_r$) even before reaching electron scales at $kd_e \geq 1$. For larger values of m_i/m_e , it extends without significant damping beyond $kd_e = 1$.

In Fig. 3, we show the dispersion relations for the FM/W wave in quasi-parallel direction of propagation. This mode shows the typical quadratic whistler-mode behaviour at $1 \lesssim kd_i \lesssim \sqrt{m_i/m_e}$. The FM/W wave is dominated by electron dynamics unless $kd_i \lesssim 1$. With decreasing m_i/m_e , ω_r/Ω_i decreases while $|\gamma|/\Omega_i$ increases. We attribute this behaviour to increasing cyclotron damping by electrons, which is, for the quasi-parallel FM/W wave, most efficient when $n = -1$ in Eq. (17). Thermal electrons with $v_{\parallel} \approx -w_e$ thus efficiently resonate with the quasi-parallel FM/W mode when

$$\left(\frac{\omega_r}{\Omega_i}\right) \approx -(kd_i) \cos \theta \sqrt{\frac{m_i}{m_e} \beta_e} + \frac{m_i}{m_e} \quad (18)$$

in our normalization. In the electron-positron case with $m_i/m_e = 1$, a significant number of electrons resonate with the FM/W mode at $\omega_r/\Omega_i = \omega_r/|\Omega_e| \lesssim 1$ and at $kd_i = kd_e \lesssim 1$ (see fig. 2 by Gary & Karimabadi 2009). Like in the case of the quasi-parallel A/IC wave, the resonant cut-off of the dispersion relation for $\omega_r \rightarrow |\Omega_e|$ is also present in the cold-plasma limit (Stix 1992). The quasi-parallel FM/W mode

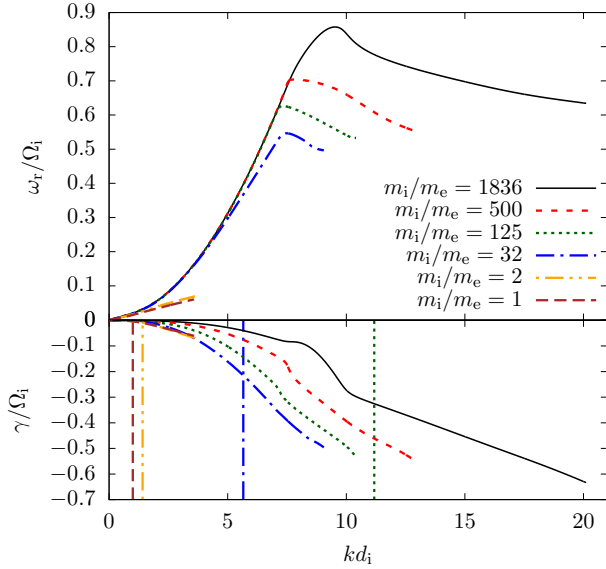


Figure 2. Dispersion relations of the A/IC wave in quasi-perpendicular propagation for different values of m_i/m_e . The light-to-Alfvén speed ratio is fixed at $c/v_{Ai} = 10^4$. The top panel shows the normalized real part of the wave frequency, and the bottom panel shows the normalized imaginary part of the wave frequency as functions of the normalized wavenumber k . The vertical lines in the bottom panel mark the positions of $kd_e = 1$ for the given mass ratios.

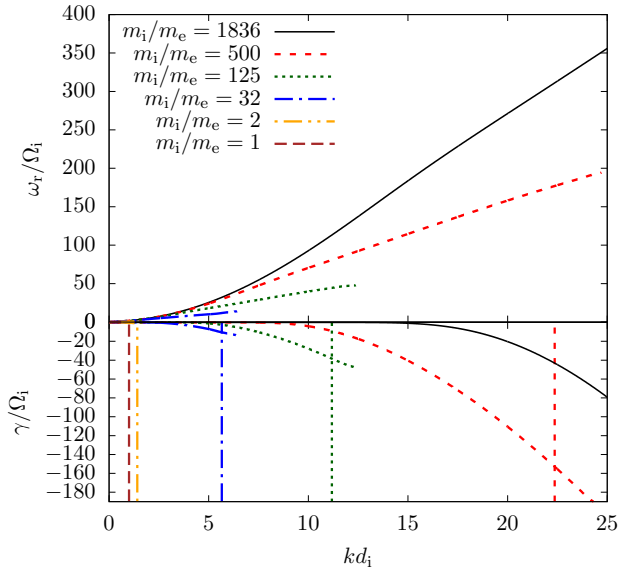


Figure 3. Dispersion relations of the FM/W wave in quasi-parallel propagation for different values of m_i/m_e . The light-to-Alfvén speed ratio is fixed at $c/v_{Ai} = 10^4$. The plot follows the same format as Fig. 2.

reaches the wavenumber range $kd_e \geq 1$ with $|\gamma| < \omega_r$ for all mass ratios shown in Fig. 3.

In Fig. 4, we show the dispersion relations for the FM/W wave in quasi-perpendicular direction of propagation. The dispersion relation does not depend significantly on m_i/m_e for $m_i/m_e \gtrsim 10$. The quasi-perpendicular FM/W

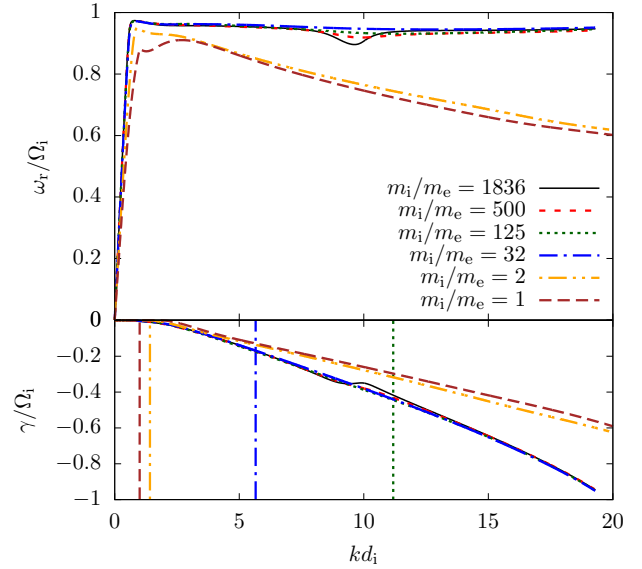


Figure 4. Dispersion relations of the FM/W wave in quasi-perpendicular propagation for different values of m_i/m_e . The light-to-Alfvén speed ratio is fixed at $c/v_{Ai} = 10^4$. The plot follows the same format as Fig. 2.

wave reaches the ion-Bernstein regime at $\omega_r/\Omega_i \approx 1$. In the perpendicular limit ($\theta \rightarrow 90^\circ$), the susceptibilities χ_j for both ions and electrons include sums over all n of contributions that are each proportional to $1/(\omega_r - n\Omega_j)$, leading to this resonant behaviour. As long as $m_i/m_e \gg 1$, electron harmonics do not interfere with the ion harmonics since the electrons' contributions to ϵ decrease with increasing n . For $m_i/m_e = 2$, however, the second-order ion resonance makes a contribution to ϵ that is comparable with the first-order electron resonance. The quasi-perpendicular FM/W mode reaches the wavenumber range $kd_e \geq 1$ with $|\gamma| < \omega_r$ for all shown parameter combinations with $m_i/m_e \leq 125$.

2.2 Dependence on light-to-Alfvén speed ratio

We now investigate the dependence of the dispersion relation on c/v_{Ai} . For this study, we fix the mass ratio at $m_i/m_e = 100$ and $m_i/m_e = 1$ (electron-positron plasma). We then vary c/v_{Ai} between 10^4 and 3 for $m_i/m_e = 100$ and between 10 and 3 for $m_i/m_e = 1$. The magnetization, therefore, varies from $|\Omega_e|/\omega_e = 10^{-3}$ to $|\Omega_e|/\omega_e \approx 3.33$ for $m_i/m_e = 100$ and from $|\Omega_e|/\omega_e = 0.1$ to $|\Omega_e|/\omega_e \approx 3.33$ for $m_i/m_e = 1$. Applying our normalization to Eq. (15) and multiplying with v_{Ai}^3/c^3 removes the c/v_{Ai} dependence from all terms in Eq. (15) except the unit tensor in the definition of ϵ in Eq. (16). This unit tensor represents the displacement current in Ampère's law, and thus c/v_{Ai} controls the effects due to the displacement current in our normalization.

Relativistic plasma effects become important if

$$\frac{k_B T_j}{m_j c^2} \gtrsim 1. \quad (19)$$

In our normalization,

$$\frac{k_B T_j}{m_j c^2} = \frac{1}{2} \beta_j \frac{m_i}{m_j} \left(\frac{v_{Ai}}{c} \right)^2. \quad (20)$$

For $\beta_j = 1$, relativistic effects, therefore, become important if

$$\frac{c}{v_{Ai}} \lesssim \sqrt{\frac{m_i}{m_j}}. \quad (21)$$

We note that relativistic effects already modify the plasma behaviour if $k_B T_j / m_j c^2 \gtrsim 0.1$. For the cases under consideration, ions do not fulfil Eq. (21)¹. Electrons, however, easily satisfy Eq. (21) even when using unrealistic mass ratios in plasma models. We, therefore, calculate the true relativistic dispersion relation with the ALPS code (Verscharen et al. 2018) for comparison with the non-relativistic solutions from NHDS. For our ALPS calculations, we assume that the plasma consists of an isotropic, non-relativistic ion species with a Maxwellian distribution function [see Eq. (14)] and an isotropic, relativistic electron species with a Jüttner distribution (Jüttner 1911),

$$f_{0j} = \frac{n_j}{2\pi m_j^3 c w_j^2 K_2(2c^2/w_j^2)} \exp\left(-2\frac{c^2}{w_j^2} \frac{1}{\sqrt{1-v^2/c^2}}\right), \quad (22)$$

where K_2 is the modified Bessel function of the second kind. We use the following parameters in our ALPS calculations (for definitions, see Verscharen et al. 2018): $c/v_{Ai} = 10$, $\beta_i = \beta_e = 1$, $m_i/m_e = 100$, $N_\perp = 100$, $N_\parallel = 200$, $N_\Gamma = 100$, $N_{\tilde{p}\parallel} = 500$, $P_{\max,\parallel i} = P_{\max,\perp i} = 10m_i v_{Ai}$, $P_{\max,\parallel e} = P_{\max,\perp e} = 0.6m_i v_{Ai}$, $J_{\max} = 10^{-45}$, $M_I = 3$, $M_P = 100$, and $t_{\text{lim}} = 0.01$. With these parameters,

$$\frac{k_B T_e}{m_e c^2} = 0.5, \quad (23)$$

corresponding to a mildly relativistic regime for the electrons, while the ions are non-relativistic.

In Fig. 5, we show the dispersion relations for the A/IC wave in quasi-parallel propagation. We see that this mode's behaviour is largely independent of c/v_{Ai} . Even for $c/v_{Ai} = 3$, its deviation from the high- c/v_{Ai} case is insignificant. We note that the A/IC wave is strongly damped at scales $kd_i \gtrsim 1$, so that potential modifications at smaller scales due to smaller c/v_{Ai} are not relevant in the propagating regime of the A/IC wave. In the quasi-parallel A/IC wave with $m_i \gg m_e$, the ions carry most of the polarization current unless $kd_i \ll 1$, in which case both ions and electrons contribute almost equally to the polarization current. Therefore, our relativistic calculation for $m_i/m_e = 100$ and $c/v_{Ai} = 10$ is almost identical to the non-relativistic case.

In Fig. 6, we show the dispersion relations for the A/IC wave in quasi-perpendicular propagation. Like in the quasi-parallel case, the c/v_{Ai} dependences of ω_r/Ω_i and γ/Ω_i are insignificant. We only find a small deviation of ω_r for $c/v_{Ai} = 3$ at $kd_i \gtrsim 4$. Figs. 5 and 6 suggest that the behaviour of the A/IC wave is largely independent of c/v_{Ai} in the non-relativistic case. However, the introduction of relativistic electrons changes the dispersion relation of the quasi-perpendicular A/IC wave at $kd_i \gtrsim 6$, leading to an increase in ω_r/Ω_i and a decrease in $|\gamma|/\Omega_i$ compared to the non-relativistic case. We associate this behaviour with relativistic modifications to the electron-pressure-gradient force,

¹ According to Eq. (3), it is possible that $v_{Ai}/c > 1$. In this case, all plasma waves have subluminal group velocities $< v_{Ai}$, so that v_{Ai} loses its meaning as the group velocity of any wave mode.

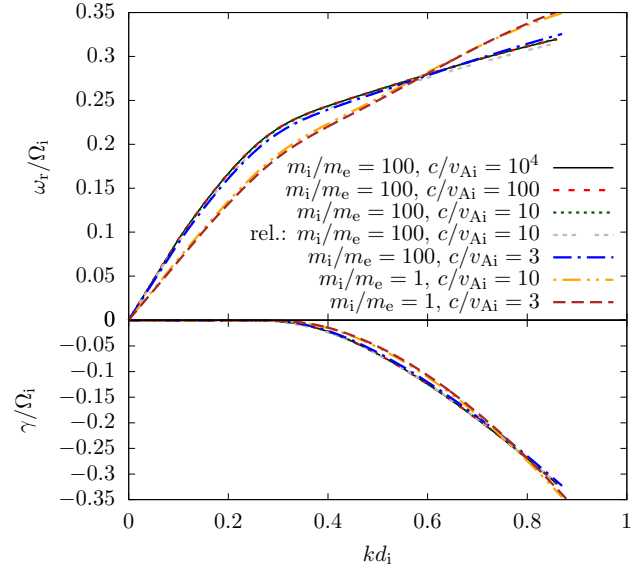


Figure 5. Dispersion relations of the A/IC wave in quasi-parallel propagation for different values of c/v_{Ai} . We fix the ion-to-electron mass ratio at $m_i/m_e = 100$ and $m_i/m_e = 1$. The top panel shows the normalized real part of the wave frequency, and the bottom panel shows the normalized imaginary part of the wave frequency as functions of the normalized wavenumber k . Only the solution marked as ‘rel.’ includes relativistic effects.

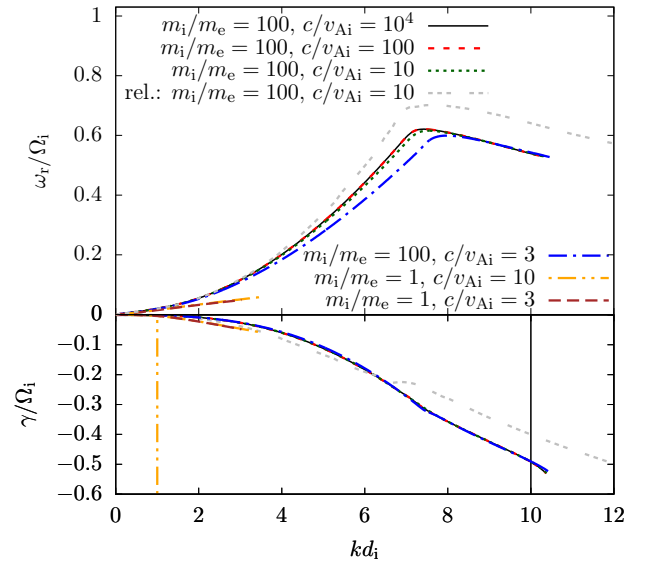


Figure 6. Dispersion relations of the A/IC wave in quasi-perpendicular propagation for different values of c/v_{Ai} . We fix the ion-to-electron mass ratio at $m_i/m_e = 100$ and $m_i/m_e = 1$. The top panel shows the normalized real part of the wave frequency, and the bottom panel shows the normalized imaginary part of the wave frequency as functions of the normalized wavenumber k . In the bottom panel, the vertical black line marks the position of $kd_e = 1$ for $m_i/m_e = 100$, and the vertical orange line marks the position of $kd_e = 1$ for $m_i/m_e = 1$. Only the solution marked as ‘rel.’ includes relativistic effects.

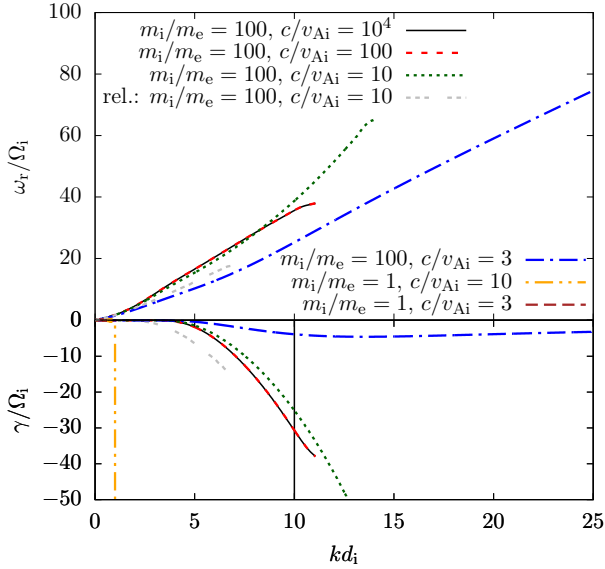


Figure 7. Dispersion relations of the FM/W wave in quasi-parallel propagation for different values of c/v_{Ai} . We fix the ion-to-electron mass ratio at $m_i/m_e = 100$ and $m_i/m_e = 1$. The plot follows the same format as Fig. 6.

which plays an important role in quasi-perpendicular A/IC waves at $k\rho_i \gtrsim 1$.

In Fig. 7, we show the dispersion relations for the FM/W wave in quasi-parallel propagation. For $c/v_{Ai} \geq 10$, the normalized dispersion relation is largely independent of c/v_{Ai} . For $c/v_{Ai} = 3$, however, the behaviour strongly deviates. We especially find that $|\gamma|/\Omega_i$ is significantly smaller than in cases with larger c/v_{Ai} . Although we clearly identify this mode as purely right-handed in polarization, it is not affected by electron-cyclotron resonant damping in the same way as the other examples. Even the FM/W-wave-typical asymptotic high-frequency behaviour at $\omega_r \approx |\Omega_e| = 100\Omega_i$ is not present. Our relativistic solution for $m_i/m_e = 100$ and $c/v_{Ai} = 10$ also deviates from our non-relativistic solution with the same parameters. Since electrons carry most of the polarization current in the quasi-parallel FM/W wave for $kd_i \gtrsim 1$, the introduction of relativistic effects leads to a slight increase in ω_r/Ω_i and a more significant increase in $|\gamma|/\Omega_i$ compared to the non-relativistic case. In the relativistic case, the cyclotron-resonance condition from Eq. (17) is modified by the relativistic mass-dependence of Ω_j :

$$\omega_r = k_{\parallel} v_{\parallel} + n\Omega_j \sqrt{1 - \frac{v^2}{c^2}}. \quad (24)$$

For a wave with fixed ω_r and k_{\parallel} , Eq. (24) suggests that v_{\parallel} is not equal for all resonant particles, as it is the case in Eq. (17). Instead, the resonance condition in Eq. (24) is fulfilled by particles with a range of v_{\parallel} , and the resonance condition now also depends on the particles' v_{\perp} through $v^2 = v_{\perp}^2 + v_{\parallel}^2$. In the relativistic case of the quasi-parallel FM/W wave, a larger number of electrons fulfil the resonance condition with $n = -1$ than in the non-relativistic case, so that $|\gamma|/\Omega_i$ increases.

In Fig. 8, we show the dispersion relations for the FM/W wave in quasi-perpendicular propagation. We find

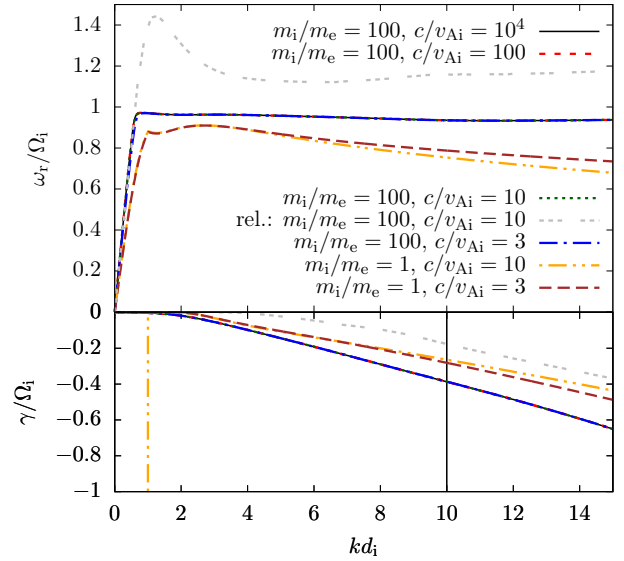


Figure 8. Dispersion relations of the FM/W wave in quasi-perpendicular propagation for different values of c/v_{Ai} . We fix the ion-to-electron mass ratio at $m_i/m_e = 100$ and $m_i/m_e = 1$. The plot follows the same format as Fig. 6.

that this mode's dispersion relation is largely independent of c/v_{Ai} for a constant value of m_i/m_e . The relativistic solution, however, shows a strong deviation from our non-relativistic solutions. For all kd_i shown in Fig. 8, $|\gamma|/\Omega_i$ is smaller than in the non-relativistic cases. However, ω_r/Ω_i is greater in the relativistic case and exhibits a local maximum near $kd_i \approx 1$. Although ion and electron scales are clearly separated in this case since $m_i \gg m_e$, relativistic electron effects modify the dispersion relation of the quasi-perpendicular FM/W wave at ion scales.

3 DISCUSSION AND CONCLUSIONS

Using linear dispersion theory, we analyse the dependence of the normalized A/IC-wave and FM/W-wave dispersion relations in quasi-parallel and quasi-perpendicular propagation on m_i/m_e and c/v_{Ai} . In nonlinear computations such as particle-in-cell and Eulerian-Vlasov simulations, these two parameters are often artificially reduced compared to their actual values in nature. This reduction enables simulations ranging from the outer scales of the system to the characteristic electron scales, which are reasonably smaller than the characteristic ion scales, while keeping computational costs small.

Using an ion normalization for frequencies and length scales, we find that the quasi-parallel A/IC wave is largely independent of m_i/m_e and c/v_{Ai} . In the quasi-perpendicular limit, m_i/m_e has a stronger effect on both the wave frequency and the damping rate of the A/IC wave than c/v_{Ai} . Relativistic effects also modify the A/IC-wave dispersion relation more strongly in the quasi-perpendicular limit than in the quasi-parallel limit. Since the electron-cyclotron resonance defines the damping of quasi-parallel FM/W waves, their behaviour strongly depends on m_i/m_e , but less so on c/v_{Ai} . Moreover, relativistic resonance effects increase the

damping rate of the quasi-parallel FM/W wave. In the quasi-perpendicular limit, the FM/W-wave dispersion relation is largely independent of m_i/m_e over a wide range of m_i/m_e . Likewise, its dispersion relation does not exhibit a strong dependence on c/v_{Ai} . We find, however, that relativistic electron effects have a strong impact on the dispersion relation of the quasi-perpendicular FM/W wave, even at ion scales.

The c/v_{Ai} dependence of all modes under consideration is small except for very small values of $c/v_{Ai} \lesssim 3$. For these small values of c/v_{Ai} , effects due to the displacement current modify the mode behaviour, especially for the quasi-parallel FM/W wave. We, therefore, recommend rather to aim for a more realistic mass ratio than for a more realistic value of c/v_{Ai} in kinetic plasma models if such a choice is necessary. There are two caveats to this conclusion: (i) relativistic effects, depending on the plasma parameters and the chosen normalization, gain importance with decreasing c/v_{Ai} ; and (ii) the scale separation between d_i and λ_i (likewise, depending on the plasma parameters and the chosen normalization, between d_e and λ_e) decreases with decreasing c/v_{Ai} , so that sub-Debye-length effects can be exaggerated at small scales when c/v_{Ai} is artificially small. Therefore, we extend our recommendation to include the consideration of unwanted relativistic and sub-Debye-length effects due to artificially low c/v_{Ai} , see Eq. (19).

Our study suggests that plasma models with $m_i/m_e \gtrsim 100$ and $c/v_{Ai} \gtrsim 10$ successfully cover physics on scales $\gtrsim 0.2d_i$ for $\beta_j \sim 1$. Our results have two implications: (i) for astrophysical plasmas composed of electron–positron pairs, the magnetization does not significantly affect the linear behaviour; and (ii) in numerical simulations of ion–electron plasmas, an artificially smaller-than-realistic mass ratio m_i/m_e affects the wave properties (frequency and damping rate) more strongly than an artificially smaller-than-realistic ratio c/v_{Ai} .

The various waves analysed here also depend on other plasma parameters such as β_j of all species, the number of species, relative drifts among them, and their temperature anisotropies (Marsch et al. 1982b,a; Kasper et al. 2002; Bale et al. 2009; Maruca et al. 2012; Verscharen et al. 2013; Yoon 2017; Klein et al. 2018). It would be useful to repeat our investigation in individual cases when using plasma models with parameters different from the representative values used in this study (Riquelme et al. 2015, 2016, 2018).

ACKNOWLEDGEMENTS

The development of the ALPS code was supported by NASA grant NNX16AG81G. D.V. is supported by the STFC Ernest Rutherford Fellowship ST/P003826/1 and STFC Consolidated Grant ST/S000240/1. T.N.P. was supported by NSF SHINE grant AGS-1460130 during the completion of this work. S.P.G. acknowledges support from NASA grant NNX17AH87G. K.G.K. acknowledges support from NASA grant 80NSSC19K0912.

REFERENCES

Allanson O., Watt C. E. J., Ratcliffe H., Meredith N. P., Allison H. J., Bentley S. N., Bloch T., Glauert S. A., 2019, *J. Geophys. Res.*, **124**, 8893

- Bale S. D., Kasper J. C., Howes G. G., Quataert E., Salem C., Sundkvist D., 2009, *Phys. Rev. Lett.*, **103**, 211101
- Boldyrev S., Horaites K., Xia Q., Perez J. C., 2013, *ApJ*, **777**, 41
- Cerri S. S., Servidio S., Califano F., 2017, *ApJ*, **846**, L18
- Cerri S. S., GroÅjelj D., Franci L., 2019, *Frontiers Astron. Space Sci.*, **6**, 64
- Cerutti B., Werner G. R., Uzdensky D. A., Begelman M. C., 2013, *ApJ*, **770**, 147
- Chen C. H. K., Boldyrev S., 2017, *ApJ*, **842**, 122
- ComiÅel H., Nariyuki Y., Narita Y., Motschmann U., 2016, *Ann. Geophys.*, **34**, 975
- Franci L., Landi S., Matteini L., Verdini A., Hellinger P., 2015, *ApJ*, **812**, 21
- Gary S. P., 1993, *Theory of Space Plasma Microinstabilities*. Cambridge University Press
- Gary S. P., Karimabadi H., 2009, *Phys. Plasmas*, **16**, 042104
- Germaschewski K., Fox W., Abbott S., Ahmadi N., Maynard K., Wang L., Ruhl H., Bhattacharjee A., 2016, *J. Comput. Phys.*, **318**, 305
- GroÅelj D., Mallet A., Loureiro N. F., Jenko F., 2018, *Phys. Rev. Lett.*, **120**, 105101
- Hasegawa A., Sato T., 2013, *Space Plasma Physics: 1 Stationary Processes*. Springer Science & Business Media
- Hunana P., Goldstein M. L., Passot T., Sulem P. L., Laveder D., Zank G. P., 2013, *ApJ*, **766**, 93
- Jüttner F., 1911, *Annalen der Physik*, **339**, 856
- Karimabadi H., et al., 2013, *Phys. Plasmas*, **20**, 012303
- Kasper J. C., Lazarus A. J., Gary S. P., 2002, *Geophys. Res. Lett.*, **29**, 1839
- Klein K. G., Howes G. G., 2015, *Phys. Plasmas*, **22**, 032903
- Klein K. G., Vech D., 2019, *Res. Not. AAS*, **3**, 107
- Klein K. G., Alterman B. L., Stevens M. L., Vech D., Kasper J. C., 2018, *Phys. Rev. Lett.*, **120**, 205102
- Kunz M. W., Stone J. M., Bai X.-N., 2014, *J. Comput. Phys.*, **259**, 154
- Lapenta G., 2012, *J. Comput. Phys.*, **231**, 795
- Markidis S., Henri P., Lapenta G., Rönnmark K., Hamrin M., Meliani Z., Laure E., 2014, *J. Comput. Phys.*, **271**, 415
- Marsch E., 2006, *Living Rev. Solar Phys.*, **3**, 1
- Marsch E., Verscharen D., 2011, *J. Plasma Phys.*, **77**, 385
- Marsch E., Rosenbauer H., Schwenn R., Muehlhaeuser K.-H., Neubauer F. M., 1982a, *J. Geophys. Res.*, **87**, 35
- Marsch E., Schwenn R., Rosenbauer H., Muehlhaeuser K.-H., Pilipp W., Neubauer F. M., 1982b, *J. Geophys. Res.*, **87**, 52
- Maruca B. A., Kasper J. C., Gary S. P., 2012, *ApJ*, **748**, 137
- Matsukiyo S., Noumi T., Zank G. P., Washimi H., Hada T., 2020, *ApJ*, **888**, 11
- Matthaeus W. H., Goldstein M. L., 1982, *J. Geophys. Res.*, **87**, 6011
- McComas D. J., et al., 2000, *J. Geophys. Res.*, **105**, 10419
- Melzani M., Walder R., Folini D., Winisdoerffer C., Favre J. M., 2014a, *A&A*, **570**, A111
- Melzani M., Walder R., Folini D., Winisdoerffer C., Favre J. M., 2014b, *A&A*, **570**, A112
- Ofman L., 2010, *Living Rev. Solar Phys.*, **7**, 4
- Opher R., 1999, *Plasma Phys. Contr. F.*, **41**, A209
- Parashar T. N., Gary S. P., 2019, *ApJ*, **882**, 29
- Parashar T. N., Salem C., Wicks R. T., Karimabadi H., Gary S. P., Matthaeus W. H., 2015a, *J. Plasma Phys.*, **81**, 905810513
- Parashar T. N., Matthaeus W. H., Shay M. A., Wan M., 2015b, *ApJ*, **811**, 112
- Pecora F., Pucci F., Lapenta G., Burgess D., Servidio S., 2019, *Sol. Phys.*, **294**, 114
- Pezzi O., et al., 2019, *J. Plasma Phys.*, **85**, 905850506
- Riquelme M. A., Quataert E., Verscharen D., 2015, *ApJ*, **800**, 27
- Riquelme M. A., Quataert E., Verscharen D., 2016, *ApJ*, **824**, 123
- Riquelme M., Quataert E., Verscharen D., 2018, *ApJ*, **854**, 132

- Roenmark K., 1982, Technical report, Waves in homogeneous, anisotropic multicomponent plasmas (WHAMP). Kiruna Geofysiska Inst., Sweden
- Roytershteyn V., Boldyrev S., Delzanno G. L., Chen C. H. K., Grošelj D., Loureiro N. F., 2019, *ApJ*, **870**, 103
- Russell C. T., 1993, *Rep. Prog. Phys.*, **56**, 687
- Saito S., Nariyuki Y., 2014, *Phys. Plasmas*, **21**, 042303
- Schekochihin A. A., Cowley S. C., Dorland W., Hammett G. W., Howes G. G., Quataert E., Tatsuno T., 2009, *ApJS*, **182**, 310
- Stix T. H., 1992, Waves in plasmas. American Institute of Physics
- Uzdensky D. A., Rightley S., 2014, *Rep. Prog. Phys.*, **77**, 036902
- Vásconez C. L., Valentini F., Camporeale E., Veltri P., 2014, *Phys. Plasmas*, **21**, 112107
- Verscharen D., Chandran B. D. G., 2018, *Res. Not. AAS*, **2**, 13
- Verscharen D., Marsch E., Motschmann U., Müller J., 2012, *Phys. Plasmas*, **19**, 022305
- Verscharen D., Bourouaine S., Chandran B. D. G., 2013, *ApJ*, **773**, 163
- Verscharen D., Klein K. G., Chandran B. D. G., Stevens M. L., Salem C. S., Bale S. D., 2018, *J. Plasma Phys.*, **84**, 905840403
- Verscharen D., Klein K. G., Maruca B. A., 2019, *Living Rev. Solar Phys.*, **16**, 5
- Wu H., Verscharen D., Wicks R. T., Chen C. H. K., He J., Nicolaou G., 2019, *ApJ*, **870**, 106
- Yoon P. H., 2015, *Phys. Plasmas*, **22**, 092307
- Yoon P. H., 2017, *Rev. Mod. Plasma Phys.*, **1**, 4
- Zhu X., He J., Verscharen D., Zhao J., 2019, *ApJ*, **878**, 48

This paper has been typeset from a $\text{\TeX}/\text{\LaTeX}$ file prepared by the author.